9.22 Nano-PIV

Contributed by:
M. Yoda

9.22.1 Background

The volume illumination used in μPIV typically gives images with low contrast, especially in the near-wall region where both reflections from the wall

Table 9.24. Nano-PIV recording parameters for electroosmotic flow through microchannels.

Flow geometry	plane parallel and adjacent to wall
Maximum in-plane velocity	$U_{\max} = 300\,\mu$m/s
Field of view	$115\,\mu\text{m} \times 15\,\mu\text{m}$
Interrogation volume	$28 \times 15 \times 0.3\,\mu\text{m}^3$ $(H \times W \times D)$
Observation distance	$z_0 < 1.5\,$mm
Recording method	multi frame, single exposure
Recording medium	intensified CCD camera
Recording lens	microscope objective ($M = 63$, $NA = 0.7$)
	camera adaptor ($NA = 0.5$)
Illumination	argon-ion laser $P \simeq 0.2\,$W
Time interval between images	$\Delta t = 5.6\,$ms
Seeding material	fluorescent polystyrene spheres
	($d_\text{p} = 100\,$nm)

and light scattered by particles beyond the focal plane contribute to the background. An alternative approach for microscale velocimetry in near-wall flows is evanescent-wave illumination. When a beam of light is incident upon a planar refractive-index interface between glass and water, for example, at an angle of incidence θ exceeding the critical angle ($\theta \simeq 63°$ for a glass-water interface), the beam will undergo total internal reflection (TIR) in the glass. Light in the form of an "evanescent wave" that is, the electromagnetic waves with complex wave number will, however, also be transmitted into the water, propagating along a direction parallel to the refractive-index interface. The intensity of these inhomogeneous waves $I \propto exp\{-z/z_p\}$ where z is the distance normal to the interface, and z_p, the (intensity-based) penetration depth, is somewhat less than the illumination wavelength [416]:

$$z_p = \frac{\lambda_0}{4\pi}\left[n_2^2 sin^2\Theta - n_1^2\right]^{-1/2}. \tag{9.5}$$

Here, n_1 and n_2 are the refractive indices of the water and glass, respectively, with $n_1 < n_2$. For illumination at visible wavelengths, the evanescent wave-illumination is therefore essentially negligible within a few hundred nanometers of the interface.

Evanescent waves can be used to illuminate the same colloidal polystyrene fluorescent spheres used in μPIV to obtain the two velocity components parallel to the wall. The resultant velocimetry technique, which we term nano-PIV (nPIV) [422], interrogates only the tracers within a very small distance – as little as 250 nm, based on tracer center position – of the wall. The spatial resolution of the technique along the optical axis (i.e., normal to the image plane) is determined by the illumination (and the camera sensitivity), and is typically significantly less than that of typical μPIV near-wall measurements which have a resolution along z of about 900 nm. Since the illumination is

restricted to such a small region, the evanescent-wave images also have less background noise than volumetrically illuminated images (cf. figure 9.105). Nano-PIV is, however, limited by the nature of evanescent-wave illumination to near-wall (vs. bulk) flow studies and hence complements the capabilities of μPIV. The near-wall capabilities of nPIV are illustrated here by a study of microscale electroosmotic flow.

9.22.2 Nano-PIV Studies of Microscale Electroosmotic Flow

Electroosmotic flow (EOF), where a conducting liquid is driven by an external electric field, is an important technology for "pumping" fluids through micro- and nanochannels. Strictly speaking, the electric field drives the fluid in a thin screening layer of counterions, known as the electric double layer (EDL), that electrostatically shields the charged wall. The characteristic length scale of the EDL, the Debye length λ_D, is less than 100 nm for most aqueous solutions. For a monovalent electrolyte solution at $298K$ [417]:

$$\lambda_D \approx \frac{0.3\,\mathrm{nm}}{\sqrt{C/(1\,\mathrm{M})}}. \tag{9.6}$$

The Debye length is therefore about 1 nm in a 0.1 M aqueous solution. It can be shown that the velocity profile is nearly uniform in a fully-developed,

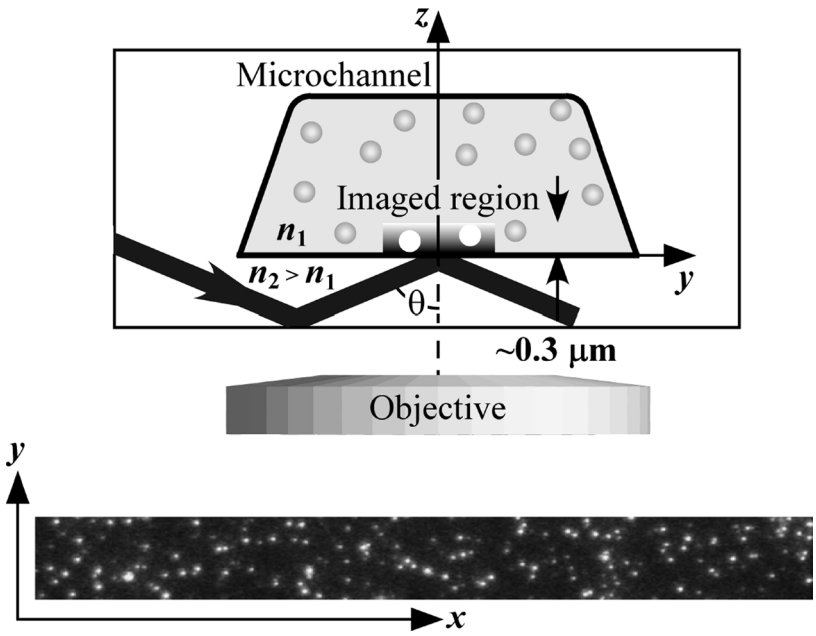

Fig. 9.105. Sketch showing the microchannel cross-section and generation of the evanescent wave using the prism method (top) and a typical image of 100 nm fluorescent polystyrene spheres illuminated by an evanescent wave at $\lambda_0 = 488\,\mathrm{nm}$ and $z_p \approx 100\,\mathrm{nm}$ (bottom). The flow direction x in the top image is out of the page. The field of view of the bottom image is about $115\,\mu\mathrm{m}\,(x) \times 12.3\,\mu\mathrm{m}\,(y)$.

one-dimensional and steady electroosmotic flow except for a very thin region next to the wall that corresponds to the EDL, the only region of the flow with nonzero charge. The extent of this "boundary layer", δ, defined as the distance from the wall where the velocity recovers to 99% of its bulk value U_{EO}, is about $4.6\lambda_D$.

The length scales required to resolve flows within the EDL have greatly limited experimental studies in this region. Both atomic force microscopy and surface forces apparatus have been used to probe the structure of the EDL in quiescent electrolyte solutions [418, 419], but such intrusive techniques cannot at present be used in most microscale EOF situations. Although the presence of a flow will not affect the EDL *per se*, surface adsorption of different electrolyte species as they are convected past the microchannel wall can greatly affect the EDL structure and hence the flow within the EDL.

Nano-PIV has been recently used to measure velocities within the EDL for very dilute aqueous solutions. Monovalent electrolyte solutions were driven by DC electric fields up to 3 kV/m through fused silica microchannels of roughly trapezoidal cross-section with nominal dimensions of $47\,\mu\mathrm{m}\,(y) \times 23\,\mu\mathrm{m}\,(x)$ (figure 9.105). The evanescent wave was generated by the TIR of an argon-ion laser beam ($\lambda_0 = 488$ nm, output power ≤ 0.2 W) at the interface between the fused silica cover slip sealing the channel and the working fluid. The penetration depth $z = 100 \pm 10$ nm, and the z-extent of the imaged region was $2.5z_p$, or about 250 nm. For this steady and fully-developed flow, the velocity in the imaged region at a given z-location should be uniform in both x and y.

The working fluid was an aqueous sodium tetraborate solution ($Na_2B_4O_7 \cdot 10H_2O$ in nano-pure water) seeded with 0.07 vol% 100 nm diameter polystyrene fluorescent spheres. The fluorescent tracers were imaged using an inverted epi-fluorescent microscope through a 63×, 0.55 NA objective and a 0.5× camera adaptor onto a CCD camera with on-chip gain at framing rates up to 178 Hz and exposures of 1 ms. A FFT correlation-based interrogation algorithm and a Gaussian peak-finding algorithm based upon a surface fit [421, 418] were used to obtain tracer displacements. Given that the flow was essentially uniform in the image plane, the interrogation windows for the second image in each pair were as large as $160\,(x) \times 68\,(y)$ pixel, *vs.* image dimensions of $653\,(x) \times 70\,(y)$ pixel. Both window shift and cross-correlation averaging over windows as small as 16×10 pixel were tested on representative data in an attempt to improve the nPIV processing, but the resultant displacements were within 2% of those obtained without window shift or cross-correlation averaging. In all cases, 1000 consecutive images were processed to obtain displacements from 999 image pairs. The results were then temporally averaged to reduce Brownian effects and, given the uniformity of the flow (based, for example, on the results from cross-correlation averaging over much smaller interrogation windows), spatially averaged as well over the entire field of view to obtain an average velocity $\overline{U}$.

Figure 9.106 shows this average velocity as a function of external electric field E for sodium tetraborate solutions at molar concentrations $C = 0.02\,\text{mM}$ (◯), 0.037 mM (△), 0.19 mM (□), 1.9 mM (◊), 3.6 mM (▽), 18.4 mM (▲) and 36 mM (×) [420]. The error bars on these data denote one standard deviation. As expected, the average velocity varies linearly with electric field, and the slope of these data is the (constant) electroosmotic mobility. For $C \geq 0.19\,\text{mM}$, equation (9.6) gives $\lambda_D \leq 22\,\text{nm}$, corresponding to $\delta < 100\,\text{nm}$, or less than half the spatial resolution of the nPIV data along z. The average velocity for these higher concentration values is therefore essentially the bulk velocity U_{EO}. At $C = 0.02$ and 0.037 mM, however, $\delta = 310$ and 230 nm, however, suggesting that these data are obtained within the EDL, and the resultant velocities should therefore be less than U_{EO}.

The nPIV results cannot be compared with known analytical predictions of the velocity profile within the EDL because of Brownian effects. The electroosmotic mobilities from the nPIV data are used instead, to validate the technique. Figure 9.107 shows μ_{ex} (◯), the mobility obtained from the data in figure 9.106 using linear regression, as a function of molar salt concentration C (the error bars on these results represent 95% confidence intervals) and analytical model predictions of the *bulk* electroosmotic mobility μ_{ex} (△) [420]. For $C \geq 0.19\,\text{mM}$, μ_{ex} and μ_∞ are within about 8% of each other. The values obtained from the nPIV data at the two lowest concentrations are, however,

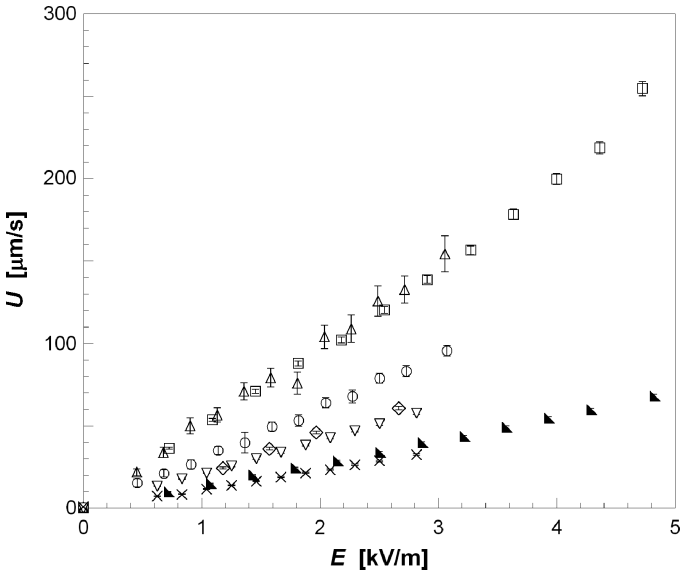

Fig. 9.106. Average velocity as a function of driving electric field for aqueous sodium tetraborate solutions at concentrations of $C = 0.02$ (◯), 0.037 (△), 0.19 (□), 1.9 (◊), 3.6 (▽), 18.4 (▲) and 36 (×) mM. The error bars represent one standard deviation.

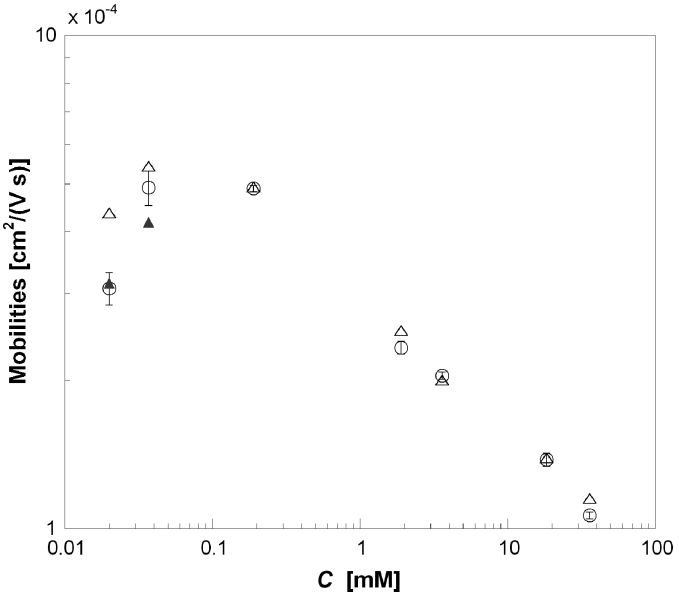

Fig. 9.107. Mobility as a function of molar concentration for aqueous sodium tetraborate solutions based on the nPIV data of figure 9.106 (◯), analytical model predictions for the bulk EOF (△), and model predictions corrected for the nonuniform velocities within the EDL (▲; only at the two lowest C). The error bars represent 95% confidence intervals for μ_{ex}.

significantly less than μ_∞, and the discrepancy is greater at $C = 0.02\,\mathrm{mM}$, as expected.

The displacements and velocities from nPIV are, strictly speaking, the tracer (*vs.* fluid) velocity. If the particle follows the flow with good fidelity, the average nPIV velocity $\overline{U}$ shown in figure 9.106 is the fluid velocity u_z averaged over the particle diameter of 100 nm. The effect of the nonuniform velocity profile within the EDL sampled by the nPIV technique on the mobility can then be estimated by averaging $\overline{U}$ over the z-extent of the region interrogated by the evanescent-wave illumination. An unweighted average then gives a correction factor:

$$\frac{u_{ex}}{u_\infty} = \frac{1}{H}\int_0^H \left[\frac{1}{d}\int_{z-0.5d}^{z+0.5d} u(z')dz'\right] dz \tag{9.7}$$

where $d = 100\,\mathrm{nm}$ is the tracer diameter and $H = 250\,\mathrm{nm}$ is the z-extent of the region sampled by the nPIV tracers. The shaded symbols at $C = 0.02$ and 0.037 mM in figure 9.107 are values for μ_∞ corrected using equation (9.7) (using the same analytical model to predict the velocity profile within the EDL).

The corrected model value and μ_{ex} differ by 3% and 15% at $C = 0.02\,\mathrm{mM}$ and $0.037\,\mathrm{mM}$, respectively. The nPIV data (unlike the model predictions) are affected by tracer electrophoresis, Brownian effects, and particle-wall EDL interactions (among other phemomena). Moreover, the nPIV tracers probably non-uniformly sample velocities within the region illuminated by the evanescent wave. Given these considerations, we consider the agreement between the experimental data and the model predictions to be acceptable.

In summary, these results illustrate some of the capabilities of evanescent wave-based particle-image velocimetry. Nano-PIV has been used to obtain what is believed to be the first experimental verification of the reduction in near-wall mobility due to the presence of the diffuse electric double layer in electroosmotic flow of an aqueous monovalent solution. The nPIV results are supported by analytical predictions. The asymmetric tracer diffusion and non-uniform illumination inherent in this technique present interesting challenges in terms of improving the accuracy and robustness of this technique.